# Project of Strategic Interest NEXTDATA

Scientific Report for the reference period 1/01/2017-31/12/2017

## Deliverable D1.5.A (June 2017)

## Report on the oceanographic cruises focused to recover marine cores and on the analysis carried out on the marine sediments (sedimentology, microfossils and isotopes), containing graphs, tables and description of the methods (Task 1)

**Resp. Fabrizio Lirer, CNR-IAMC**

Lirer Fabrizio[1], Alberico Ines[1], Bonomo Sergio[1], Cascella Antonio[2], Di Rita Federico[3], Ferraro Luciana [1], Florindo Fabio[4], Insinga Donatella Domenica[1], Lurcock Pontus Conrad [4], Magri Donatella[3], Margaritelli Giulia[1], Pelosi Nicola[1], Vallefuoco Mattia[1]

1) Istituto per l'Ambiente Marino Costiero (IAMC) – Consiglio Nazionale delle Ricerche, Calata Porta di Massa, Interno Porto di Napoli, 80133, Napoli, Italia
2) Istituto Nazionale di Geofisica e Vulcanologia (INGV), Via della Faggiola 32, 52126 Pisa, Italia
3) Dipartimento di Biologia Ambientale – Botanica, Università La Sapienza di Roma, Piazzale Aldo Moro 5, 00185 Roma, Italia
4) Istituto Nazionale di Geofisica e Vulcanologia (INGV), Via di Vigna Murata 605, 00143 Roma, Italia

The research activities related to Deliverable D1.5A of project include the data acquired during the oceanographic cruise NEXTDATA-2016 aboard the CNR R/V Minerva Uno. During this oceanographic cruise, new marine sedimentary cores have been recovered in different sectors of the Ionian Sea, Sicily Channel and the whole Tyrrhenian Sea, within a joint scientific activity with two international research groups (Isabel Cacho of University of Barcelona and Marie-Alexandrine Sicre of Locean-CNRS Paris). In particular, during this oceanographic cruise, 43 marine cores (using Kullenberg and SW104 gravity corer systems), 21 hydrographic stations and 12 Multinet plankton sampler transects for living planktonic foraminifera, were recovered (Fig. 1a, 1b, 1c and Tab. 1, see supplementary materials).

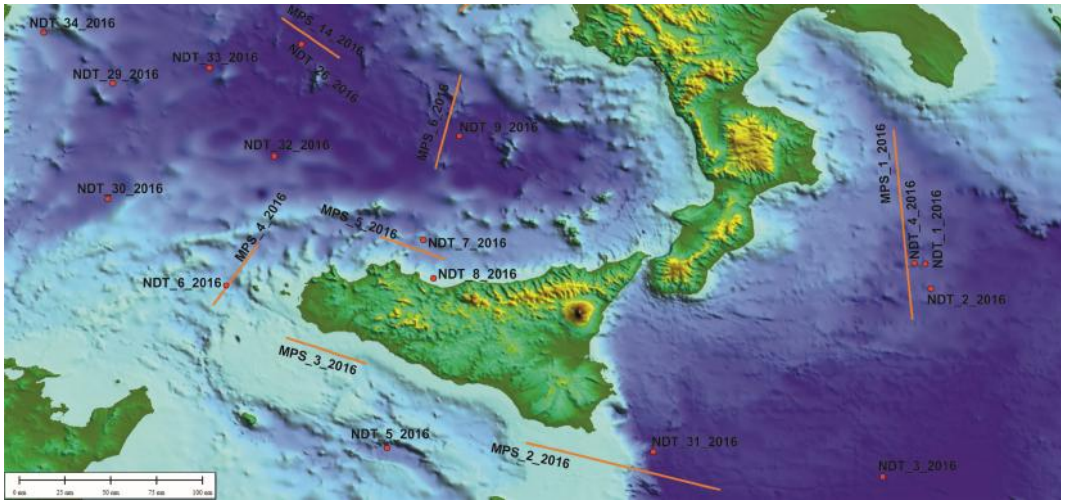


Figure 1a – Location map of cores (red point) and Multinet plankton sampler transects (orange lines)

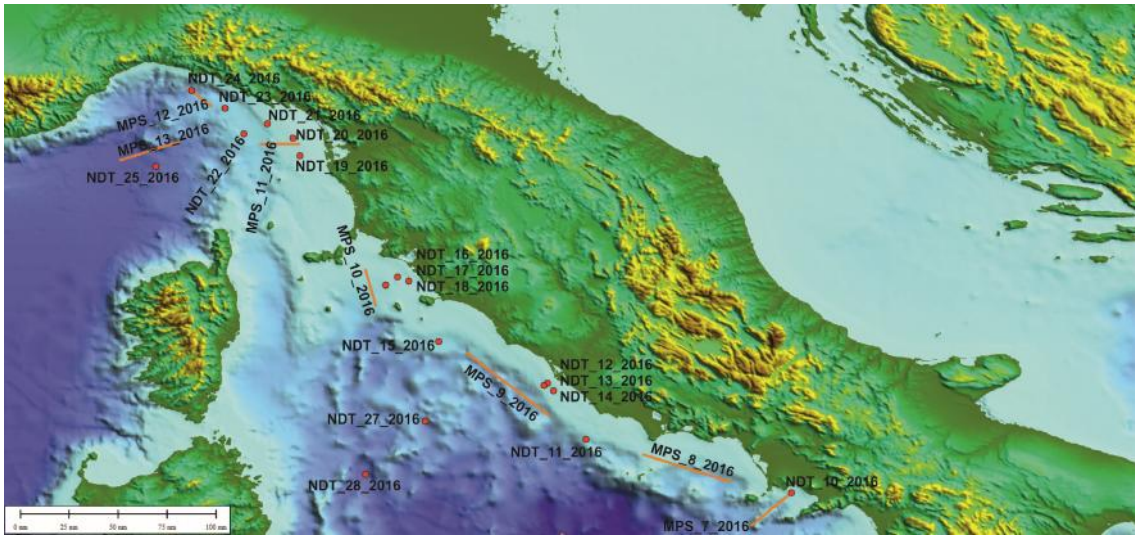


Figure 1b – Location map of cores (red point) and Multinet plankton sampler transects (orange lines)

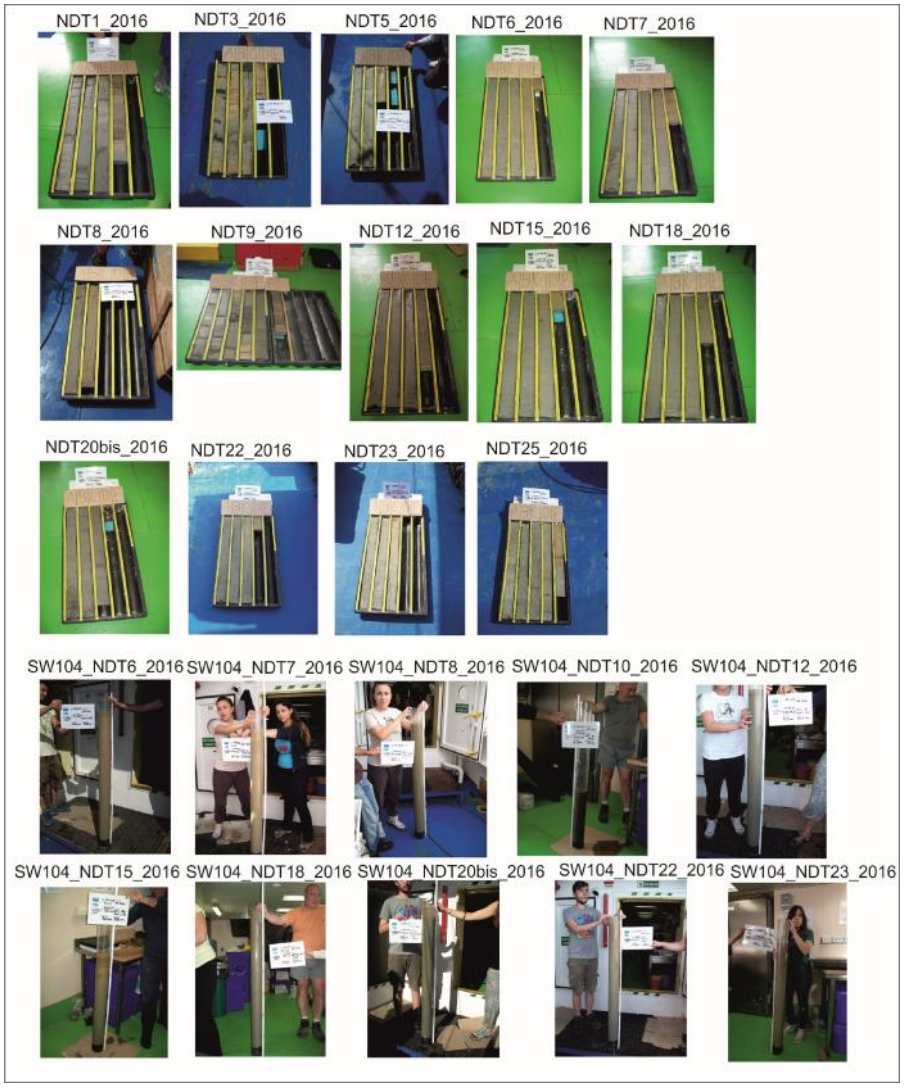


Figure 1c – Photos of marine cores recovered during NEXTDATA2016 oceanographic cruise

Some of this sites have been studied for planktonic foraminifera (SW104-NDT-18_2016, North Tyrrhenian Sea; SW104-NDT-8_2016, south Tyrrhenian Sea at North Sicily Island) to identify decadal climatic oscillation over the last millennium, allowing to produce a complete framework of the climatic variability documented during the last millennium in the Tyrrhenian Sea (Dentici PhD thesis, 2018).

In addition, a total of 133 water samples, collected with Niskin bottles, were recovered in 21 hydrographic stations (Fig. 2). To investigate the total thickness of the photic zone, seven depth levels (5, 25, 50, 75, 100, 150 and 200 meters) were selected.

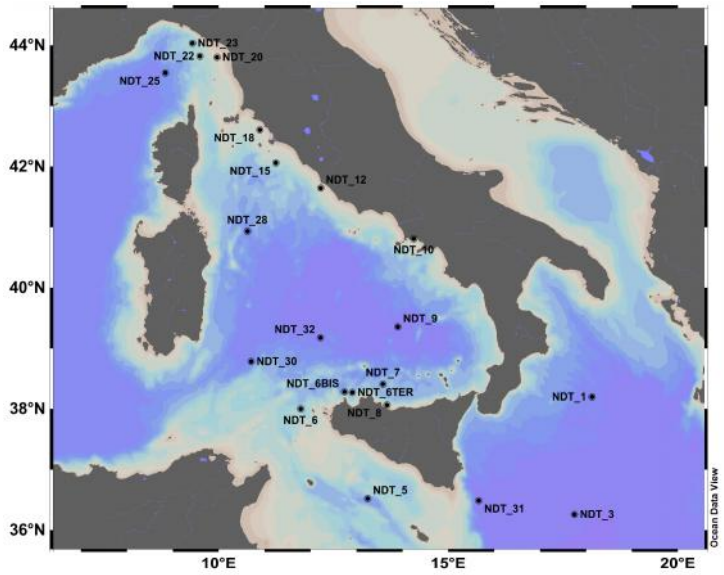

Figure 2 – Investigated area, location of stations where CTD profiles and Coccolithophore data were collected.

During cruise, coccolithophore production was found significantly higher only in the central part of the investigated area (Fig. 3), possibly because of the presence of a weakened and shallower thermocline. Relatively low productivity from the Ligurian Sea is not surprising under the light of the peculiar behaviour of this region within the Mediterranean context. In fact, this area, located east to the Gulf of Lions, is characterized by spring bloom, occurring when sea surface waters are calmer but still nutrient enriched. Blooms start in April and last about six weeks, culminating in early May (Morel and André, 1991; Cacho et al., 1999; D'Ortenzio, 2003).

Taxa grouped in the Upper Photic Zone (UPZ) group are K-strategists, specialized to live in warm subtropical surface waters and to exploit a minimum amount of nutrients (Okada and Mcintyre, 1979; Roth and Coulbourne, 1982; Takahashi and Okada, 2000; Andruleit et al., 2003; Boeckel and Baumann, 2004; Baumann et al., 2005). Coherently with this ecological niche, UPZ taxa have been found in relative high abundance during cruise (Fig. 3). They are significantly abundant in the upper part of the water column in presence of a deep summer thermocline, as especially evident for relative abundances. According to Knappertsbusch (1993), on the basis of investigation on surface sediments and by comparison of western and eastern Mediterranean sedimentary archives, species referred to the UPZ group are thought to show a marked West-East gradient, with higher abundance in the easternmost sector, which follows the change in nutrient availability. This trend is clear evident during the NextData2016 cruise (Fig. 3).

The Lower Photic Zone (LPZ) group (and its most important species, *Florisphaera profunda*) (Fig. 3), is related to a complex interplay of environmental factors. It is restricted to the lower photic zone (Okada and Honjo 1973; Jordan and Winter 2000) and lives below the thermocline, under low light and temperature conditions (Molfino and McIntyre 1990; Winter et al. 1994; Young 1994b; Takahashi and Okada 2000; Winter et al. 2002; Malinverno et al. 2003). In the studied area, this group increases its abundance at 100-150 m depth and constitutes the typical deep coccolithophore assemblage.

Finally, one of the most interesting result of the NextData 2016 cruise coccolithophorids data is associated with the distribution of *Gephyrocapsa* spp. This species seems to be confined to the Sicilian Channel and displays a good correspondence with the salinity minimum of the MAW flux, almost virtually disappearing at the entrance of the Ionian Sea, which might act as an ecological barrier (Fig. 3). Such a consideration opened intriguing scenarios on the use of this taxon as a paleoceanographic proxy for surface waters of Atlantic origin and for evaluating possible incursions of this water mass into the eastern Mediterranean basin.

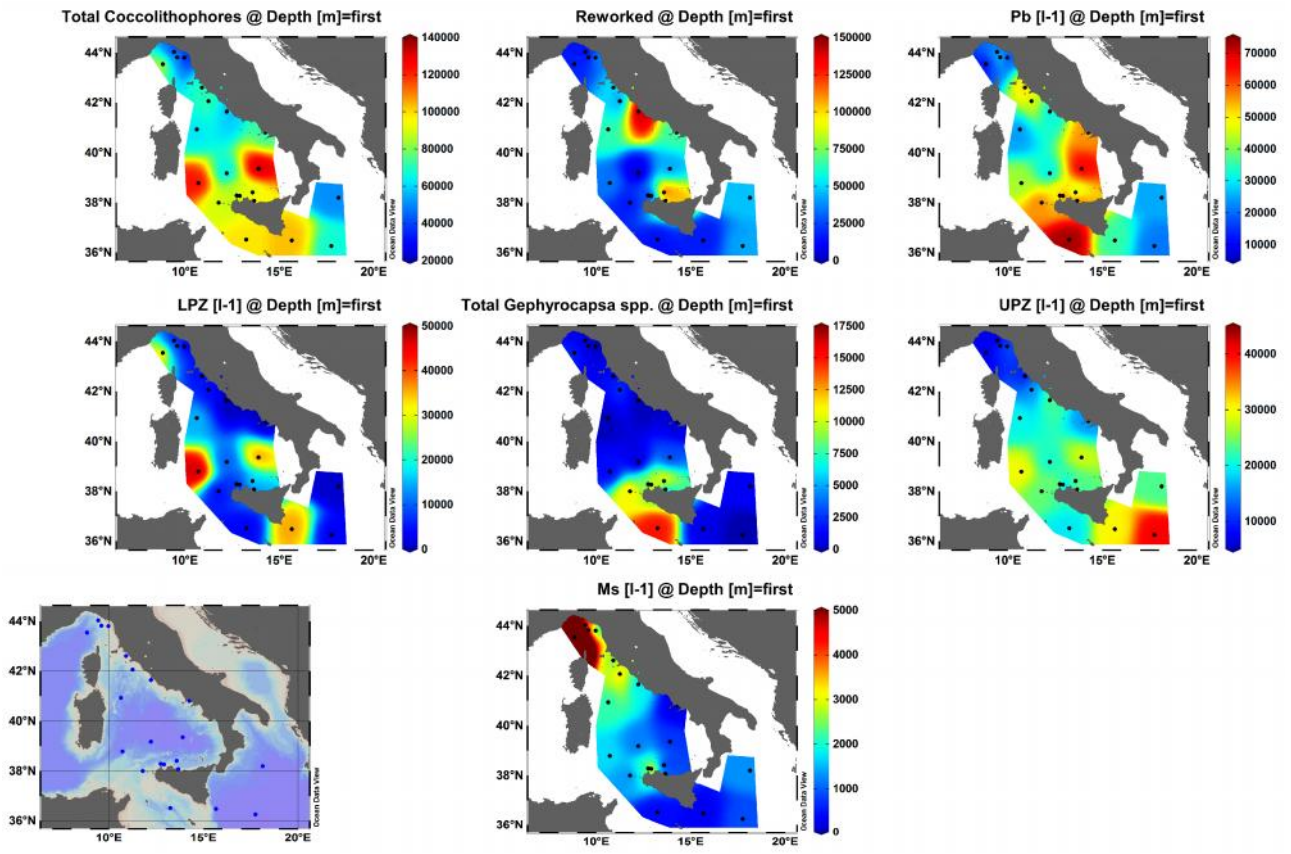


Figure 3 – Surface maps (5 m depth) of the concentrations of the Total Coccolithophores, reworked taxa, Total Gephyrocapsa spp. and the 4 differentiated ecological groups (cel l-1) (Pb: Placolith-bearing taxa – UPZ: Upper Photic Zone taxa – LPZ: Lower Photic Zone taxa – Ms: Miscellaneous taxa) in water samples across the studied area.

Concerning the Grand challenges of NEXTDATA project, the high-resolution studies focused on last millennia and carried out on selected key-sites of the western Mediterranean basin, allowed us to identify and date important intervals associated with archaeological/cultural periods: Eneolithic, Early Bronze Age, Middle Bronze Age–Iron Age, Roman Period, Dark Age, Medieval Climatic Anomaly, Little Ice Age, Industrial Period and Modern Warm Period (Margaritelli et al. 2016). These intervals mark important change in past climate oscillation over the last four millennia those strongly control the response of planktonic foraminifera (base level of food web) (Margaritelli et al. 2016) and pollen contents (Di Rita et al. 2018) in the Mediterranean. In particular, Margaritelli et al. (2016) documented that following the cooling phase related to the cold 2.8 kyr event (Bond cycle 2), from beginning of the Roman Period (ca. 500 BCE) upwards, the climate system displays a turnover *vs* a more positive NAO index, associated with a long-term trend to lower $\delta^{18}O_{G.ruber}$ values and with a significant planktonic foraminiferal changes from carnivorous *vs* herbivorous-opportunistic species (Fig. 4). The herbivorous-opportunistic species are the dominant group over most of the last two millennia, suggesting a strong connection with nutrient availability.

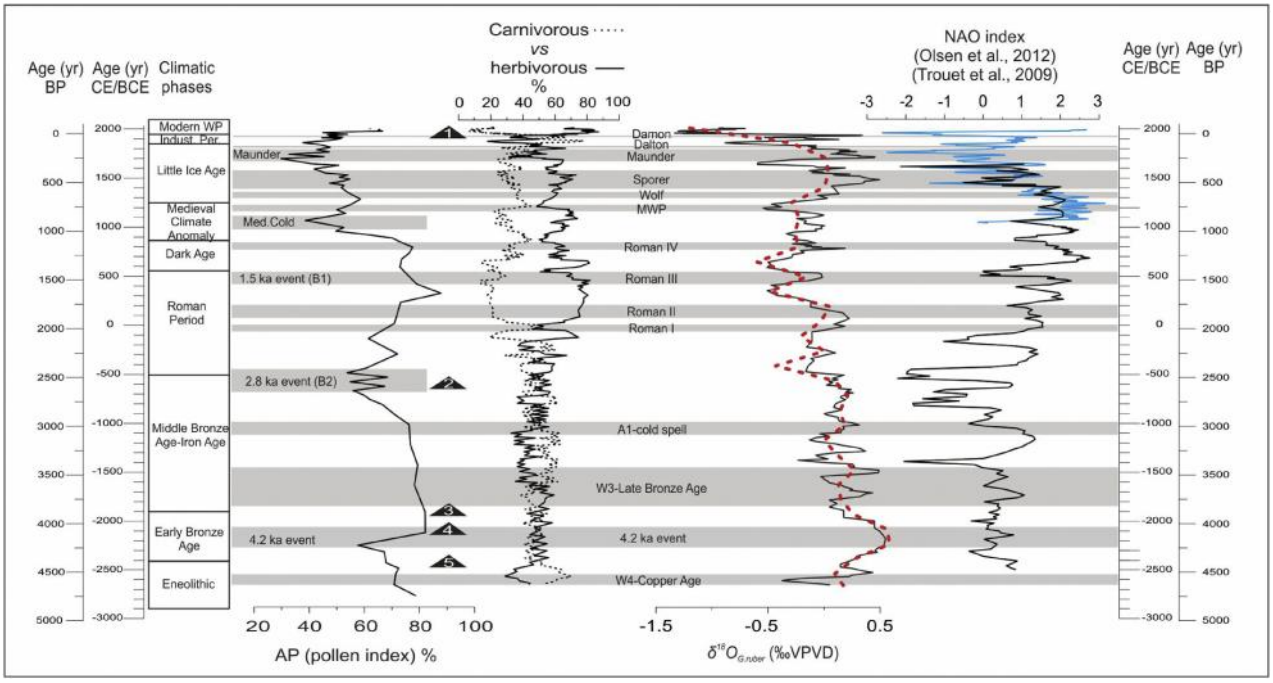


Figure 4 – Comparison in time domain between the AP pollen data index, planktonic foraminiferal turnover (carnivorous vs herbivorous–opportunistic species), $\delta^{18}$Osignal (5 point moving average black line and 150 years moving average thick red dotted line) and NAO index (black line by Olsen et al., 2012; blue line by Trouet et al., 2009). The grey bands represent the identified climatic events. The labels 2.8 ka event (B2) and 1.5 ka event (B1) correspond to the position of Bond events 1 and 2 (Bond et al., 2001). The label Med. cold corresponds to Medieval cold. Modern WP = Modern Warm Period; Indust. Per. = Industrial Period. The black triangles with the number from 1 to 5 are the position of the identified tephra layers: 1—Vesuvius (1906 CE), 2—Vateliero–Ischia (2.4–2.6 ka BP), 3—Capo Miseno (3.9 ka BP), 4—Astroni3 (4.1–4.3 ka BP), 5—Agnano M. Spina (4.42 ka BP).

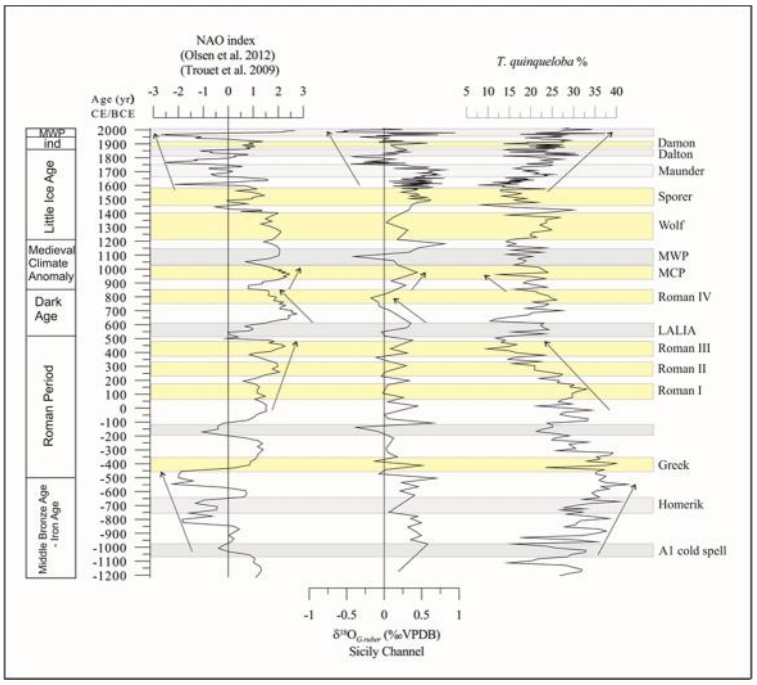


Figure 5 – Comparison between NAO index reconstruction (Trouet al., 2009; Olsen et al., 2012), δ18OG.ruber signal and *Turborotalita quinqueloba* from core SW104-ND2-ND2 (east Sicily Channell, Dentici PhD thesis 2018).

As documented by Bonomo et al. (2016), Margaritelli et al. (2016) and Di Rita et al. (2018), the North Atlantic Oscillation (NAO) index represents one of the main factors controlling the internal variability of climate change over the last millennia in the Mediterranean. In particular, in Italy, the NAO index modulates the winter precipitation (Brunetti et al., 2002; Tomozeiu et al., 2002; Caloiero et al., 2011; López-Moreno et al., 2011; Casanueva et al., 2014; Benito et al.,

2015) following a opposite trend with respect to the northern Europe (López-Moreno et al., 2011; Benito et al., 2015; and references therein). Within this framework, Dentici PhD thesis (2018) proposed the comparison between NAO index (Trouet et al., 2009; Olsen et al., 2012), the planktonic foraminifer *Turborotalita quinqueloba*, assumed considered as proxy of seasonal flooding events and/or high surface productivity (e.g. Vallefuoco et al., 2012; Margaritelli et al., 2016; Di Rita et al., 2018) and $\delta^{18}O_{G.\ ruber}$ signal. In particular, *T. quinqueloba* results in antiphase with NAO index (Fig. 5), documenting a strong forcing of NAO index also in the east Sicily Channel.

The sea surface Mediterranean $\delta^{18}O_{G.ruber}$ records correlation among different regions of the Mediterranean Sea over the last three millennia (Margaritelli et al. *submitted Palaeogeography, Palaeoclimatology, Palaeoecology*) allowed us to verify the synchronicity of climate events in land and ocean in order to better understand global forcing within the Mediterranean region (Fig. 6). Notwithstanding differences in time resolution and age control, we underline a general good agreement between long and short term-trends in sea surface Mediterranean $\delta^{18}O_{G.ruber}$ records (Fig. 6) during the last 2700 years. In particular, in the upper part of the Dark Age, the prominent cooling event associated to the Roman IV solar minima, marks the beginning of a progressive cooling trend that culminates during the LIA (Fig. 6), in agreement with the climate signal deduced by tree-rings (Büntgen et al., 2016). This climate perturbation is well documented in the $\delta^{18}O_{G.ruber}$ records of western and eastern Mediterranean Sea, as well as in the north Europe continental records (PAGES 2K Consortium, 2013). It results to be almost synchronous with an increase in amplitude change in solar activity ($\Delta$14C, Stuiver et al., 1998) and progressive shift vs negative NAO index (Trouet et al., 2009; Olsen et al., 2012) (Fig. 6). A new short-term cooling phase (between 536 to ca. 630 AD), recently defined by Büntgen et al. (2016) as Late Antique Little Ice Age (LALIA) could be considered as an additional environmental factor marking an important change in human culture and defining a possible trigger for political, societal and economic turmoil. At the contrary, rather temperate climate conditions characterize the MCA as documented by marine (Schilman et al., 2001, Grauel et al., 2013; Lirer et al., 2014; Cisneros et al., 2016; Margaritelli et. al., 2016) and terrestrial paleo-archives (Büntgen et al., 2016). During this time interval, $\delta^{18}O_{G.ruber}$ records and foraminiferal data document mild climate conditions with a short-term cold dry event (MCP – Medieval cold period) at ca. 1050 CE characterized by a decrease in arboreal vegetation in the central Tyrrhenian area (Margaritelli et al., 2016; Di Rita et al., 2018). The MCA period was coincident with the climax of many Mediterranean cultures. During the twelfth century, the medieval Byzantine Empire went through an important societal expansion, with substantial agricultural productivity, intensive monetary exchange, demographic growth, and its pre-eminent international political situation (Xoplaki et al., 2015).
The establishment of colder conditions in the climate system from ca. 1200 CE upwards characterized the entire LIA as provided by temperature reconstructions (PAGES 2K Consortium, 2013; Cisneros et al., 2016) and by abrupt oscillation in Mediterranean $\delta^{18}O_{G.ruber}$ records .

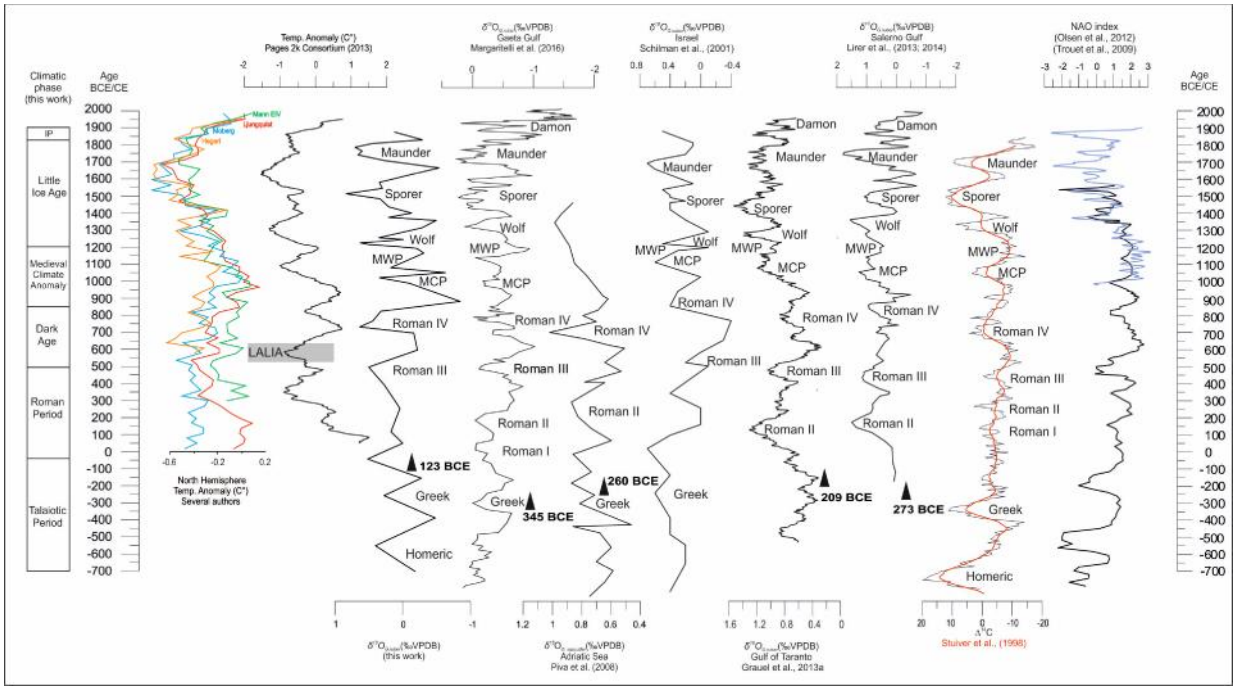


Figure 6 – Comparison in time domain between North Hemisphere mean temperatures reconstruction from different authors [Moberg et al., 2005 (blue curve); Hegerl et al., 2006, 2007 (yellow curve); Mann et al., 2008 (green curve); Ljungqvist et al., 2010 (red curve)], Temperature anomaly (C°) (Pages 2k Consortium, 2013), δ18OG.ruber (‰VPDB) of Menorca core (this study), δ18OG.ruber (‰VPDB) of Gulf of Gaeta (Margaritelli et al., 2016), δ18OG.ruber (‰VPDB) of Gulf of Salerno (Lirer et al., 2013; 2014); δ18OG.ruber (‰VPDB) of Gulf of Taranto (Grauel et al., 2013), δ18OG. sacculifer (‰VPDB) of Adriatic Sea (Piva et al., 2008), δ18OG.ruber (‰VPDB) of Israel (Schilman et al., 2001), Δ14C (Stuiver et al., 1998) and NAO index (black line by Olsen et al., 2012; blue line by Trouet et al., 2009). The acronym MWP corresponds to Medieval Warm Period, MCP to Medieval Cold Period and LALIA to the Late Antique Little Ice Age proposed by Büntgen et al. (2016). The black arrows with ages represent the ages when this areas becomes part of the Roman Impere.

To support the hypothesis of a synchronous response of Mediterranean marine sediments to past climate changes, we provide the correlation between planktonic foraminiferal paleoclimatic curves obtained from different environmental areas of Mediterranean basin (Fig. 7). Notwithstanding differences in time resolution and age control, this correlation permits to verify the almost synchronous response of planktonic foraminifera to global climate events, and allow us throughout the correlation with NAO index and Δ14C residual to better understand global forcing within the Mediterranean region (Fig. 7).

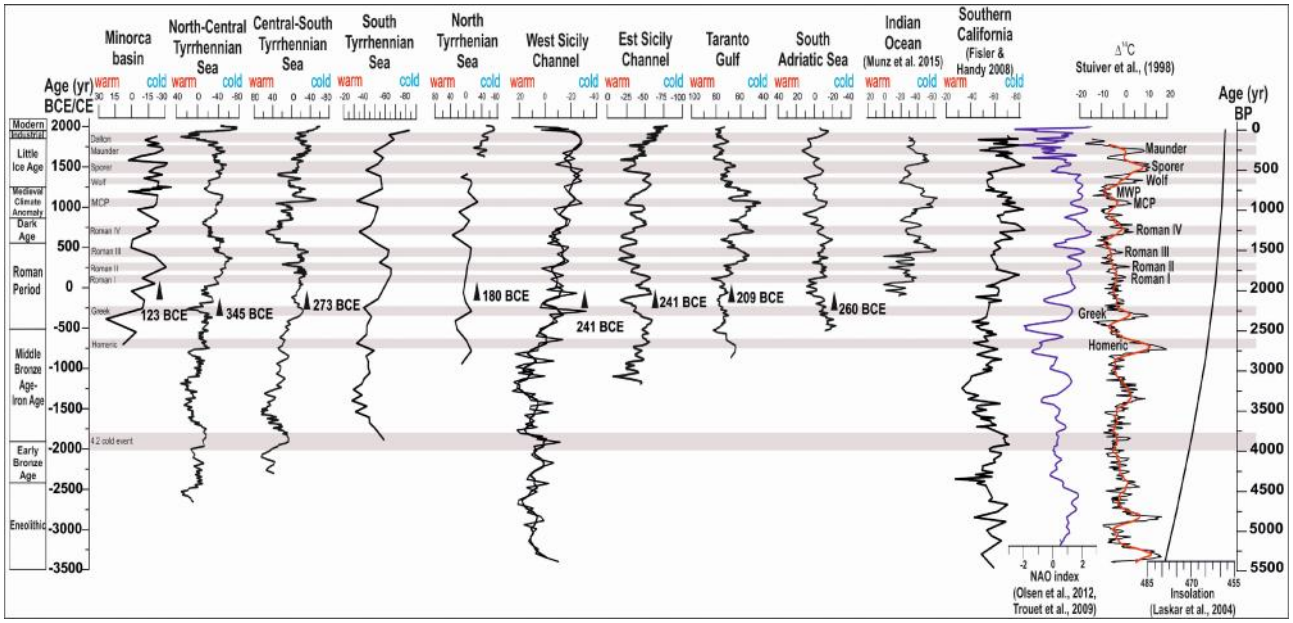


Figure 7 – Comparison in time domain between planktonic foraminiferal paleoclimatic curves obtained from different environmental areas of Mediterranean basin: i) Minorca Basin (Margaritelli et al. submitted), ii) north-central Tyrrhenian Sea

(Margaritelli et al., 2016), iii) Central-South Tyrrhenian Sea (Lirer et al., 2013; 2014), iv) South Tyrrhenian Sea (Dentici PhD thesis, 2018), v) west Sicily Channel (Margaritelli et al. in prep), vi) east Sicily Channel (Dentici PhD thesis, 2018), vi) Gulf of Taranto (Margaritelli PhD thesis, 2016), vii) South Ionian Sea (Lirer et al. in prep), viii) Indian Ocean (Munz et al., 2015), ix) southern California (Fisler and Handy 2008) and NAO index (Olsen et al., 2012 and Trouet et al., 2009), Δ14C (Stuiver et al. 1998) and Isolation (Laskar et al., 2004). The light grey bands indicate the cold phases. The black arrows with ages represent the ages when this areas becomes part of the Roman Impere

In particular, the planktonic foraminiferal paleoclimatic curves document an overall warm and stable climatic condition from 3500 BCE to 750 BCE, corresponding to a low amplitude oscillation in Δ14C residual and to a period where NAO index does not show particular trend and/or main oscillation. From 750 BCE to ca. 250 BCE, the Mediterranean and extra-Mediterranean paleoclimatic curves document a transition-cooling phase, which becomes consistent in correspondence of the sharp global cooling related to Homeric solar minimum (at ca. 250 BCE). This short time interval corresponds to the well-known Sterno-Etrussia excursion in terrestrial magnetic field (Dergachev et al. 2004) connected with solar activity decrease (Homeric minimum) which should be accompanied by increased transfer of wet Atlantic air to the east (Dergachev et al. 2004). The global cooling over the last two millennia, related to the decrease in insolation, is documented by the parallelism of all planktonic foraminiferal paleoclimatic curves, showing an isochronous response of Mediterranean and extra-Mediterranean planktonic foraminifera. Discrepancy with Taranto Gulf and South Adriatic Sea records may be related to local overprint and/or local oceanographic condition.
This long-term cooling trend results parallel to a progressive trend vs negative anomaly in Δ14C residual as well as parallel to the shift of NAO index trend toward positive values and reach the maximum cooling during the Little Ice Age at ca. 1800 CE (Maunder Minimum). At ca. 550 CE the planktonic foraminiferal paleoclimate curves show a further cooling phase, which age corresponds to the Late Antique Little Ice Age (LALIA), considered as an additional environmental factor contributing to the establishment important change in human culture. At 1800 CE, the paleoclimatic curves show a turnover vs the modern warm climate condition. This effort will provide a more complete high-resolution picture about the climate changes in the Mediterranean region and the validity of planktonic foraminifera as tool for global paleoclimate reconstruction over the last five millennia.

Concerning the time interval of last 500 years, the extremely high sedimentation rate of core SW104-NDT18_2016 in the north Tyrrhenian Sea, in from of Ormbrone river, allowed us to document decadal oscillation in planktonic foraminiferal paleoclimatic curve and $\delta^{18}O_{G.\ ruber}$ signals (Dentici PhD thesis, 2018) (Fig. 8). In particular, it is clearly evident a progressive cooling trend from 1400 (Wolf solar minimum event) to beginning of Industrial Period in paleoclimatic curve. Upwards the paleoclimatic curve shows a shift vs warm climate condition. The $\delta^{18}O$ *G. ruber* record resembles the paleoclimatic curve signal documenting the beginning of warm climate condition at ca. 1930 CE. This datum fits with the increase in global atmospheric temperature anomaly by instrumental data.

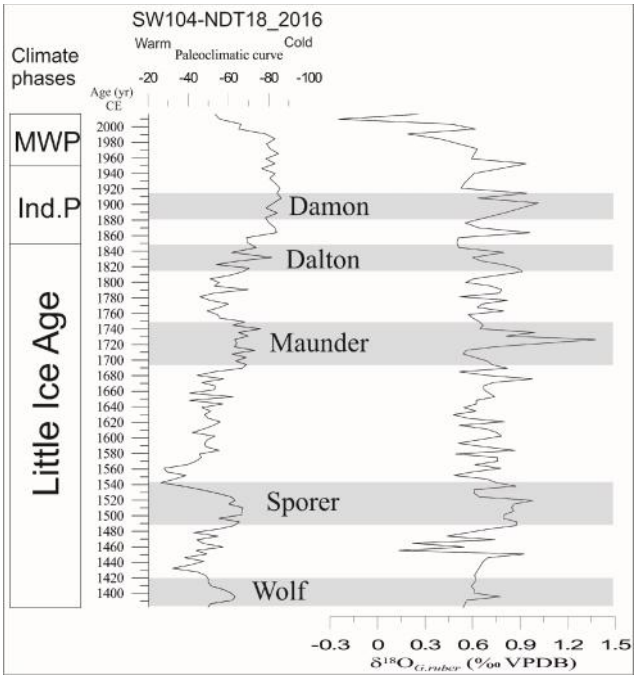


Figure 8 – Comparison in time domain between planktonic foraminiferal paleoclimatic curve and $\delta^{18}O_{G.\ ruber}$ of core SW104-NDT18_2016 (Dentici PhD thesis, 2018) from North Tyrrhenian Sea (Ombrone river).

In term of forest dynamics over the last millennia in the Mediterranean region and the timing and development of cultivations in southern Italy, De Rita et al. (2018) provided novel insights into the vegetation response to climate variability, and raises new questions about the mechanisms of past atmospheric circulation patterns in the central Mediterranean Basin. The Authors have found a clear correspondence between phases with negative (positive) NAO index and forest declines (increases). This suggests that in the southern-central Mediterranean negative NAO conditions are associated with cold/dry events, and vice-versa (Fig. 9).
In particular, we have found the following openings of vegetation coeval with climate changes reported by independent proxies:

- Around 4200 cal BP, a drop in AP, especially evergreen oaks, in the Gaeta record confirms the forest decline recorded in many sites in Italy south of 43N, and parallels a phase of declining NAO values, culminating around 4250 cal BP. This may correspond to decreasing winter precipitations, determining a reduction of evergreen vegetation.
- Around 2800 cal BP, a vegetation change towards open conditions is found in the Gaeta record, which is not clearly discussed in other pollen records from the region, although vegetation changes are visible in several sites. The NAO index clearly shows negative values. As in the case of the 4.2 ka event, this phase may correspond to a decrease in winter precipitation in the central-southern Mediterranean, matching the "Bond 2" cold event recorded in the North Atlantic (Bond et al., 2001). This time interval corresponds also to a decrease in solar activity (Martìn-Puertas et al., 2012).
- Between 800 and 1000 AD, a remarkable forest decline is represented in the Gaeta record, coeval with a decrease in the frequencies of both Castanea and Olea. The oxygen isotope record from the Gaeta core shows a shift towards positive values indicating cooler temperatures. The NAO index reconstructions (Wassenburg et al., 2013; Baker et al., 2015) once again point to a generally negative index circulation pattern.
- Between 1400e1850 AD, in the time period chronologically corresponding to the LIA, the Gaeta record shows a clear decline of the forest cover particularly evident after 1550 AD, mainly at the expense of the evergreen forest belt, suggesting dry climate conditions. In the same core, both the planktonic foraminifera assemblages and the oxygen stable

isotope indicate a change towards a colder climate. As in the preceding openings of the forest, the NAO index shows negative values.

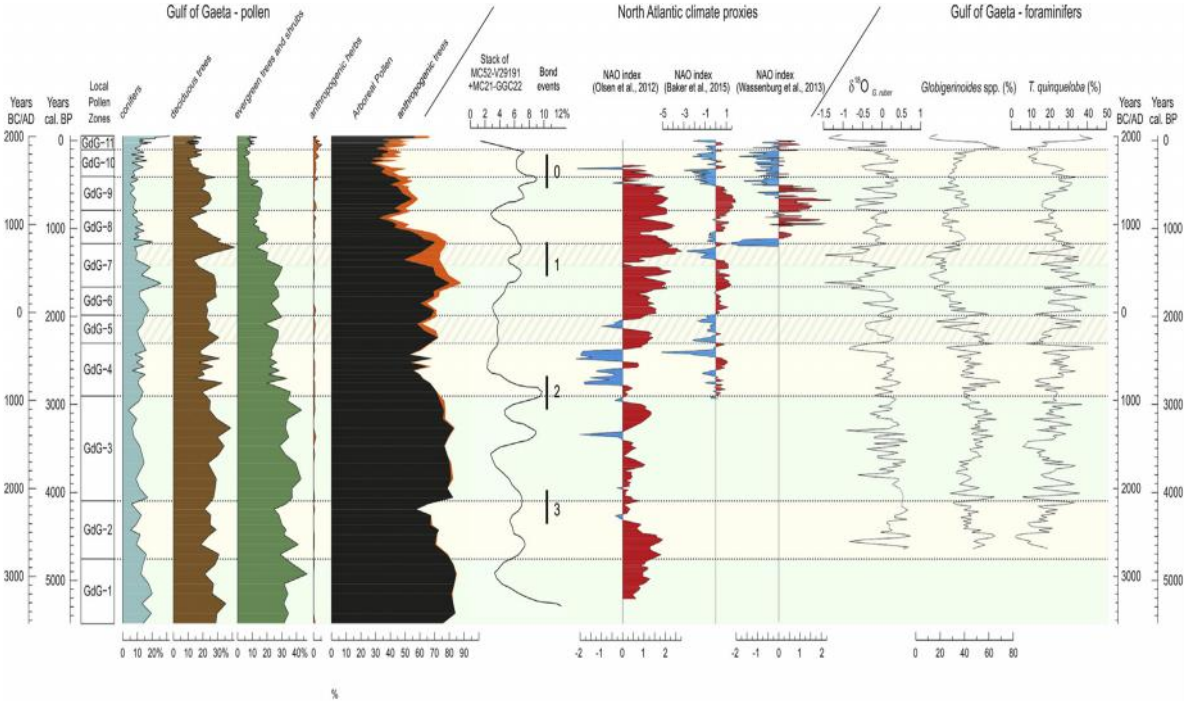


Figure 9 – Summary pollen percentage diagram including the cumulative percentages of conifers (mostly represented by Pinus, Juniperus, and Abies), riparian trees (Alnus, Salix, Populus, and Tamarix), deciduous trees (mostly deciduous Quercus, Corylus, Fagus, Ostrya/Carpinus orientalis, Carpinus betulus and Ulmus), evergreen trees and shrubs (evergreen Quercus, Ericaceae, Phillyrea, and Pistacia), anthropogenic indicators (including Castanea, Olea, and other cultivated and anthropochore taxa such as Juglans, Vitis, cereals, etc.), Arboreal Pollen (Arboreal Pollen þ Anthropogenic trees), $\delta\ ^{18}O_{G.\ ruber}$, the *Globigerinoides* total % and *Turborotalita quinqueloba* % plotted with 5-point moving average from the Gulf of Gaeta (SW104-C5-C5), chronologically correlated with proxies of the "Bond events" (Bond et al., 2001), and the NAO index reconstructed by Olsen et al. (2012), Wassenburg et al. (2013), and Baker et al. (2015).

Phases with positive NAO index values generally match periods of forest expansion (Fig. 9). In particular, between 4100 and 2900 cal BP there is a remarkable increase of both evergreen and deciduous trees. Similar extensive forests are also found in many other sites in the Central Mediterranean (Di Rita and Magri, 2012 and references therein). A second time interval with forest expansions matching a positive NAO index, from ca. 50 BC to 600 AD, includes the Roman Imperial period and the beginning of the Middle Ages. In spite of massive human activity, witnessed also by abundant anthropogenic indicators in the pollen record, stable forest conditions were probably favoured by a humid climate. A third period with a relative forest development within a generally open anthropogenic landscape is found between approx. 1050 and 1550 AD, at a time when all NAO index reconstructions indicate positive values (Olsen et al., 2012; Wassenburg et al., 2013; Baker et al., 2015).

Concerning the Sea Surface Temperature (SST) anomaly reconstruction in the Mediterranean marine record over the last millennia, Cisneros et al. (2016) produced the first SST stack using Mg/Ca ratio measured on planktonic foraminifer *Globigerina bulloides* from Minorca basin (western Mediterranean). The construction of a robust chronological framework in the region allows for the synchronization of the different core sites and the construction of "stacked" proxy records in order to identify the most significant climatic variability patterns (Fig. 10). The warmest sustained period occurred during the Roman Period (RP), which was immediately followed by a general cooling trend interrupted by several centennial-scale oscillations. We propose that this general cooling trend could be controlled by changes in the annual mean insolation.

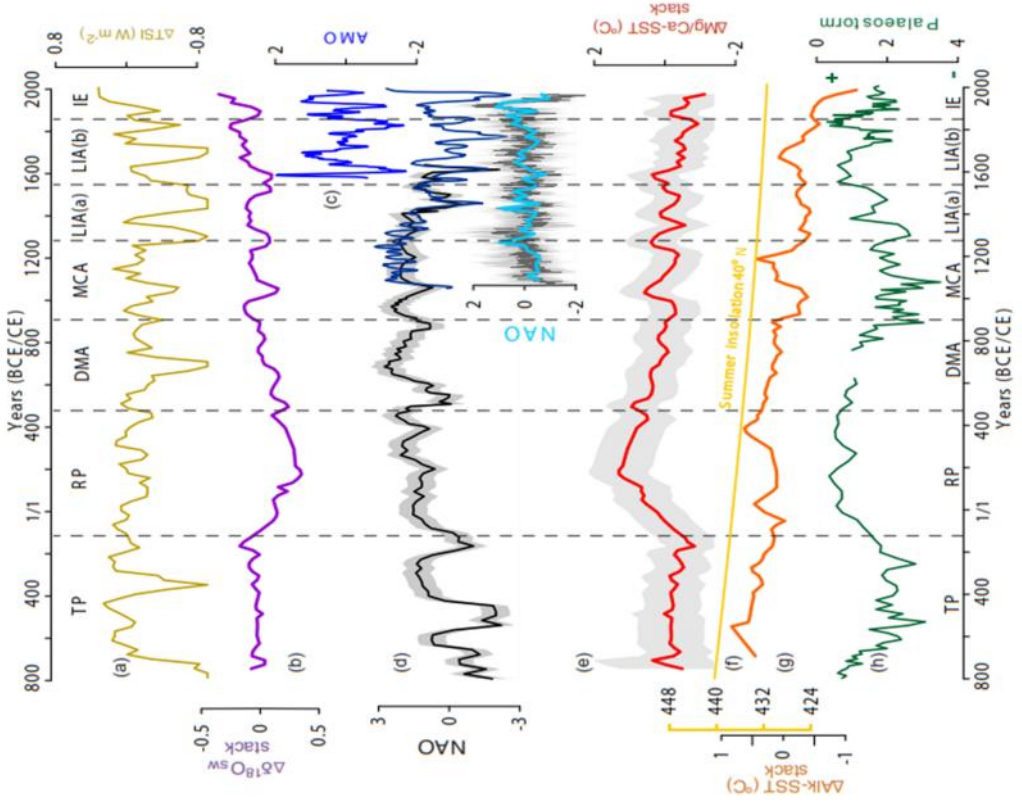


Figure 10 – Temperature and isotope anomaly records from Minorca (this study) and data from other regions and with external forcings: (a) total solar irradiance (Steinhilber et al., 2009, 2012), (b) Minorca stacks, (c) Atlantic Multidecadal Oscillation (AMO; Gray et al., 2004), (d) North Atlantic Oscillation (NAO) reconstructions (Olsen et al., 2012; Trouet et al., 2009; and, for the last millennium, Ortega et al., 2015), (e) Mg/Ca–SST anomaly Minorca stack, (f) summer insolation at 40N (Laskar et al., 2004), (g) alkenone–SST anomaly Minorca stack, and (h) palaeostorm activity in the Gulf of Lion (Sabatier et al., 2012).

To provide a more complete framework of SST anomaly over the last millennia in the Mediterranean basin Margaritelli et al. (in prep) produced the first SST Mg/Ca anomaly reconstruction measured on planktonic foraminifer *Globigerinoides ruber* from western part of Sicily Channel (core SW104-ND11). This record has been compared with the Mg/Ca *Globigerina bulloides* anomaly stack of Menorca basin (Cisneros et al., 2016) and with SST Uk37 anomaly reconstruction from Aegean Sea (Kotthoff et al., 2008). This comparison allowed us to document for the first time a prominent warm interval characterised by a shift of ca. 2°C *vs* positive anomaly (Fig. 10). This well pronounced warm interval from 100 yr BCE to 500 CE occurs during the Roman Period. This SST evolution during the Roman Period is consistent with the isotopic record of the Gulf of Taranto (Goudeau et al., 2015) and with other records from northern Europe (Bond et al., 2001; Sicre et al., 2008; Esper et al., 2014) and with the continental anomaly reconstruction from Europe (PAGES 2K, 2013). However, none of these records highlights the Roman times as the warmest climate period of the last 2 kyr. Despite the different ecological niche of the planktonic foraminiferal species used to reconstruct the Mg/Ca ratio for the Sicily Channel (*G. ruber*) and the Menorca Basin (*G. bulloides*), this warming phase is recognisable in both records. In addition, this warm phase during the Roman Period is also recorded in the SST Uk37 SST anomaly reconstruction from Aegean Sea (Kotthoff et al., 2008), documenting the occurrence of a Mediterranean global event (Fig. 10). It is possible to speculate that this long-term warming phase had a major role in the rise of Roman civilization.

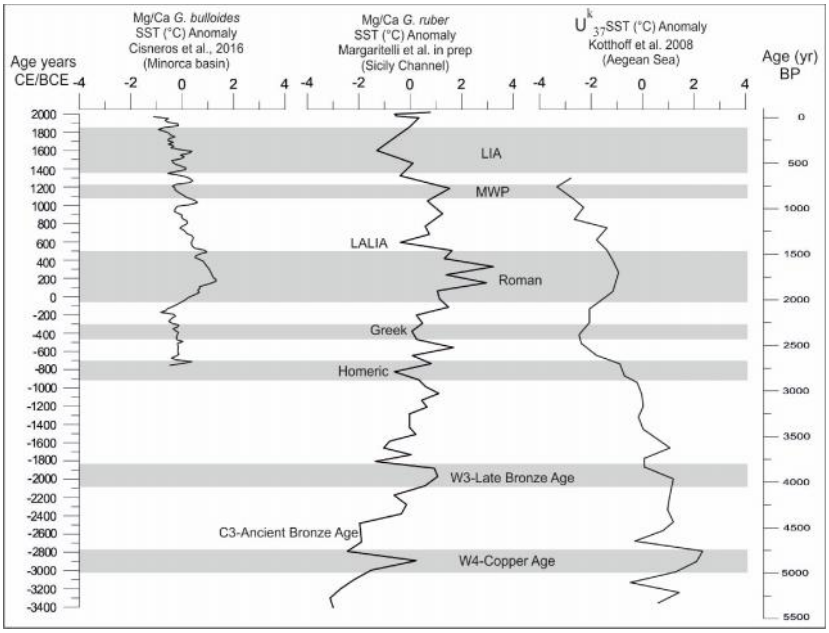


Figure 10 – Comparison in time domain between SST Mg/Ca *G.ruber* (core SW104-ND11, Sicily Channel, Margaritelli PhD thesis 2016), SST Mg/Ca *G.bulloides* (Minorca basin, Cisneros et al., 2016) and SST Uk37 SST (Aegean Sea, Kotthoff et al., 2008). The grey bands shows the main climate events documented in the Mediterranean basin.

In addition, the new SST Mg/Ca *G. ruber* anomaly reconstruction from Sicily Channel, documented the short-term cooling phase associated with the Late Antique Little Ice Age (LALIA) event at ca. 600 CE (Dark Age) and the well-known Medieval Warm Period at ca. 1200 CE (Fig. 10). Upwards, the cooling associated to the Little Ice Age event occurs between 1320 CE and ca. 1850 CE with an anomaly of ca. 2°C *vs* negative values.

Scientific articles published in NextData project:

Lirer, F., Sprovieri, M., Vallefuoco, M., Ferraro, L., Pelosi, N., Giordano, L., Capotondi, L., (2014). Planktonic foraminifera as bio-indicators for monitoring the climatic changes occurred during the last 2000 years in the SE Tyrrhenian Sea. *Integrative Zoology*, 9: 542–554. doi: 10.1111/1749-4877.120

Capotondi L., Girone A., Lirer F., Bergami C., Verducci M., Vallefuoco M., Afferri A., Ferraro L., Pelosi N., De Lange G. J., (2016). Central Mediterranean Mid-Pleistocene paleoclimatic variability and its connection with global climate. *Palaeogeography, Palaeoclimatology, Palaeoecology*, 442, 72-83, doi: 10.1016/j.palaeo.2015.11.009

Cisneros M., Cacho I., Frigola J., Canals M., Masqué P., Martrat B., Casado M., Grimalt J., Pena L. D., Margaritelli G. and Lirer F., (2016). Sea surface temperature variability in the central-western Mediterranean Sea during the last 2700 years: a multi-proxy and multi-record approach. *Clim. Past*, 12, 849–869, doi:10.5194/cp-12-849-2016

Margaritelli G., Vallefuoco M., Di Rita F., Capotondi L., Bellucci L.G., Insinga D.D., Petrosino P., Bonomo S., Cacho I., Cascella A., Ferraro L., Florindo F., Lubritto C., Lurcock P.C., Magri D., Pelosi N., Rettori R., Lirer F., (2016). Marine response to climate changes during the last five millennia in the central Mediterranean Sea. *Global and Planetary Change*. 142, 53-72. doi: 10.1016/j.gloplacha.2016.04.007.

Bonomo S., Cascella A., Alberico I., Sorgato S., Pelosi N., Ferraro L., Lirer F., Vallefuoco M., Bellucci L., Agnini C., Pappone G., (2016). Reworked Coccoliths as runoff proxy for the last 400 years: The case of Gaeta Gulf (central Tyrrhenian Sea, Central Italy). *Palaeogeography, Palaeoclimatology, Palaeoecology* 459, 15–28

Marra, F., Rohling, EJ, Florindo, F., Jicha, B., Nomade, S., Pereira, A., Renne, PR. (2016). Independent 40 Ar/39 Ar and 14 C age constraints on the last five glacial terminations from the aggradational successions of the Tiber River, Rome (Italy). Earth and Planetary Science Letters 449, 105-117, http://dx.doi.org/10.1016/j.epsl.2016.05.037

Alberico I., Giliberti I., Insinga D.D., Petrosino P., Vallefuoco M., Lirer F., Bonomo S., Cascella A., Anzalone E., Barra R., E. Marsella, and Ferraro L., (2017). Marine sediment cores database for the Mediterranean Basin: a tool for past climatic and environmental studies. Gruyter *Open Geoscience*, 9; 221–239.

Marra, F., Florindo, F., Jicha, B., (2017). 40Ar/39Ar dating of Glacial Termination VI: constraints to the duration of Marine Isotopic Stage 13, Scientific Reports - Nature. http://www.nature.com/articles/s41598-017-08614-6

Marra, F., Florindo, F., Petronio, C., (2017). Quaternary fluvial terraces of the Tiber Valley: geochronologic and geometric constraints on the back-arc magmatism-related uplift in central Italy, Scientific Reports - Nature. www.nature.com/articles/s41598-017-02437-1.
Marra, F., Luberti, G.M., Florindo, F., (2017). A review of the stratigraphy of Rome (Italy) according to geochronologically and paleomagnetically constrained aggradational successions, glacio-eustatic forcing and volcano-tectonic processes, Quaternary International. http://dx.doi.org/10.1016/j.quaint.2017.01.044
Di Rita F., Lirer F., Bonomo S., Cascella A., Ferraro L., Florindo F., Insinga D., Lurcock P., Margaritelli G., Petrosino P., Rettori R., Vallefuoco M., Magri D., (2018). Late Holocene forest dynamics in the Gulf of Gaeta (central Mediterranean) in relation to NAO variability and human impact. *Quaternary Science Reviews*, 179; 137-152

## Scientific articles submitted to ISI journal in NextData project:

Jalali B., Sicre M.A., Klein V., Schmidt S., Maselli V., Lirer F., Bassetti M.-A., Toucanne S., Jorry S. J., Insinga D., Petrosino P., Châles F. (submitted to *Paleoceanography*). Deltaic and coastal sediments as recorders of Mediterranean regional climate and human impact over the past millennia
Lurcock P., Florindo F., Margaritelli G., Vallefuoco M., Di Rita F., Insinga D.D., Petrosino P., Bonomo S., Cascella A., Ferraro L., Magri D., Pelosi N., Cosentino C., Lirer F., (submitted to *JGR-Solid Earth*). A 4,500-year record of paleosecular variation and relative paleointensity from the Tyrrhenian Sea.
Di Rita F., Fletcher W. J., Aranbarri J., Margaritelli G., Lirer F., Magri D., (submitted to *Scientific Reports*). Holocene forest dynamics in central and western Mediterranean: periodicity, spatio-temporal patterns and climate influence
Margaritelli G., Cisneros M., Cacho I., Capotondi L., Vallefuoco M., Rettori R., Lirer F., (submitted to *Palaeogeography, Palaeoclimatology, Palaeoecology*). Climatic variability from the Talaiotic Period to the Present in the central-western Mediterranean Sea (Menorca Basin) detected by planktonic foraminifera and stable isotope records.

| Station name | Data | Latitudine | Longitudine | Depth (m) | Magnetic Susceptbility | CTD | Multy plankton sampler (MPS) | Water sample depth | Recovery (meter) | Section |
|---|---|---|---|---|---|---|---|---|---|---|
| NDT_1_2016 (BIS) | 12/06/16 | N38°11'55.41 | E18°7'44.75 | 2711 | X | X | X (MPS1) | NDT_1_2016 depth 25 m | 3,82 m | A-D |
| | | | | | | | | NDT_1_2016 depth 85 m | | |
| | | | | | | | | NDT_1_2016 depth 200 m | | |
| | | | | | | | | NDT_1_2016 depth 300 m | | |
| | | | | | | | | NDT_1_2016 depth 800 m | | |
| | | | | | | | | NDT_1_2016 depth 2718 m | | |
| NDT_3_2016 | 13/06/16 | N36°15'36,85 | E17°44'59,17 | 3620 | X | X | | NDT_3_2016 depht 40 m | 3,36 m | A-D |
| | | | | | | | | NDT_3_2016 depht 130 m | | |
| | | | | | | | | NDT_3_2016 depht 200 m | | |
| | | | | | | | | NDT_3_2016 depht 280 m | | |
| | | | | | | | | NDT_3_2016 depht 800 m | | |
| | | | | | | | | NDT_3_2016 depht 3611 m | | |
| NDT_31_2016 | 14/06/16 | N36°29'16,84 | E15°39'53,73 | 3218 | | X | X (MPS2) | NDT_31_2016 depht 25 m | | |
| | | | | | | | | NDT_31_2016 depht 50 m | | |
| | | | | | | | | NDT_31_2016 depht 90 m | | |
| | | | | | | | | NDT_31_2016 depht 140 m | | |
| | | | | | | | | NDT_31_2016 depht 350 m | | |
| | | | | | | | | NDT_31_2016 depht 3200 m | | |
| NDT_5_2016 (BIS) | 15/06/16 | N36°31'17,70 | E13°14'40,19 | 1688 | X | X | | NDT_5_2016 depht 75 m | 2,4 m | A-C |
| | | | | | | | | NDT_5_2016 depht 120 m | | |
| | | | | | | | | NDT_5_2016 depht 300 m | | |
| | | | | | | | | NDT_5_2016 depht 1668 m | | |
| MPS_3_2016 | 15/06/16 | N37°18'16,10 | E13°00'28,70 | | | | X (MPS3) | | | |
| NDT_8_2016 BIS | 17/06/16 | N38°03'57,73 | E13°39'57,90 | 120 | X | X | | NDT_8_2016 depht 5 m | 1,95 m | A-B |
| NDT_8_2016 replica | 17/06/16 | N38°03'57,73 | E13°39'57,90 | 120 | X | X | | NDT_8_2016 depht 5 m | 1,73 m | A-B |
| | | | | | | | | NDT_8_2016 depht 25 m | | |
| | | | | | | | | NDT_8_2016 depht 50 m | | |
| | | | | | | | | NDT_8_2016 depht 75 m | | |
| | | | | | | | | NDT_8_2016 depht 100 m | | |
| | | | | | | | | NDT_8_2016 depht 120 m | | |
| NDT_8_2016 SW104 | 17/06/16 | N38°03'58,07 | E13°39'57,82 | 120 | X | X | | | 1,22 m | |
| NDT_8_2016 SW104 replica | 17/06/16 | N38°03'58,07 | E13°39'57,82 | 120 | X | X | | | 1,24 m | |
| NDT_7_2016 | 17/06/16 | N38°24'41,47 | E13°34'34,31 | 1493 | X | X | | NDT_7_2016 depht 20 m | 4,45 m | A-E |
| | | | | | | | | NDT_7_2016 depht 75 m | | |
| | | | | | | | | NDT_7_2016 depht 150 m | | |
| | | | | | | | | NDT_7_2016 depht 280 m | | |
| | | | | | | | | NDT_7_2016 depht 1474 m | | |
| NDT_7_2016 SW104 | 17/06/16 | N38°24'41,84 | E13°34'35,89 | 1493 | X | | | (Acqua interfaccia) | 1,21 m | |
| NDT_7_2016 SW104 replica | 17/06/16 | N38°24'41,84 | E13°34'35,89 | 1493 | | | | | 1,20 m | |
| MPS_5_2016 | 17/06/16 | N38°14'29,04 | E13°45'34,52 | 1493 | | | X | | | |
| NDT_9_2016 | 18/06/16 | N39°21'24,32 | E13°54'02,66 | 3359 | X | X | | NDT_9_2016 depht 25 m (6) | 5,70 m | A-F |
| | | | | | | | | NDT_9_2016 depht 95 m | | |
| | | | | | | | | NDT_9_2016 depht 400 m | | |
| | | | | | | | | NDT_9_2016 depht 900 m | | |
| | | | | | | | | NDT_9_2016 depht 1500 m | | |
| | | | | | | | | NDT_9_2016 depht 3497 m | | |
| MPS_6_2016 | 18/06/16 | N39°22'30 | E13°45'48,04 | 3332 | | | X | | | |
| NDT_10_2016 | 18/06/16 | N40°48'33,09 | E14°14'56,44 | 76 | | X | | NDT_10_2016 depht 5 m | | |
| | | | | | | | | NDT_10_2016 depht 25 m | | |
| | | | | | | | | NDT_10_2016 depht 50 m | | |
| | | | | | | | | NDT_10_2016 depht 68 m | | |
| NDT_10_2016 SW104 | 18/06/16 | N40°48'33,09 | E14°14'56,44 | 76 | X | | | (Acqua interfaccia) | 0,63 m | |
| NDT_10_2016 SW104 replica | 18/06/16 | N40°48'33,09 | E14°14'56,44 | 76 | | | | | 0,33 m | |
| MPS_7_2016 | 18/06/16 | N40°38'04,05 | E14°02'07,37 | 560 | | | | | | |
| MPS_8_2016 BIS | 19/06/16 | N41°05'49,59 | E14°00'03,14 | 1100 | | | X | | | |
| NDT_12_2016 | 19/06/16 | N41°38'47,12 | E12°13'19,27 | 100 | X | X | | NDT_12_2016 depht 5 m | 3,78 m | A-D |
| | | | | | | | | NDT_12_2016 depht 25 m | | |
| | | | | | | | | NDT_12_2016 depht 50 m | | |
| | | | | | | | | NDT_12_2016 depht 75 m | | |
| | | | | | | | | NDT_12_2016 depht 92 m | | |
| NDT_12_2016 SW104 | 19/06/16 | N41°38'47,61 | E12°13'19,89 | 100 | X | | | (Acqua interfaccia) | 1,29 m | |
| NDT_12_2016 SW104 replica | 19/06/16 | N41°38'47,61 | E12°13'19,89 | 100 | | | | | | |
| NDT_15_2016 | 19/06/16 | N42°03'39,93 | E11°14'44,96 | 386 | X | X | | NDT_15_2016 depht 40 m | 3,22 m | A-D |
| | | | | | | | | NDT_15_2016 depht 240 m | | |
| | | | | | | | | NDT_15_2016 depht 360 m | | |
| NDT_15_2016 SW104 | 19/06/16 | N42°03'39,99 | E11°14'44,76 | 386 | X | X | | (Acqua interfaccia) | 0,96 m | |
| NDT_15_2016 SW104 replica | 19/06/16 | N42°03'39,94 | E11°14'44,72 | 386 | | | | | 1,10 m | |
| NDT_18_2016 | 20/06/16 | N42°36'27,96 | E10°53'47,70 | 110 | X | X | | NDT_18_2016 depht 100 m(5) | 3,50 m | A-D |
| | | | | | | | | NDT_18_2016 depht 75 m (4) | | |
| | | | | | | | | NDT_18_2016 depht 50 m (3) | | |
| | | | | | | | | NDT_18_2016 depht 25 m (2) | | |
| | | | | | | | | NDT_18_2016 depht 5 m (1) | | |
| NDT_18_2016 SW104 | 20/06/16 | N42°36'28,10 | E10°53'48,01 | 109 | X | X | | (Acqua interfaccia) | 1,34 m | |
| NDT_18_2016 SW104 replica | 20/06/16 | N42°36'28,14 | E10°53'47,65 | 109 | | | | | 1,37 m | |
| MPS_10_2016 BIS | 20/06/16 | N42°24'12,76 | E10°36'45,94 | 451 | | | X | | | |
| MPS_11_2016 BIS | 20/06/16 | N42°28'32,86 | E09°46'27,88 | 418 | | | X | | | |
| NDT_20_2016 BIS | 21/06/16 | 43°48'11,53 | 09°57'54,31 | 73 | X | X | | NDT_20_2016 BIS depht 5 m | 2,90 m | A-C |
| | | | | | | | | NDT_20_2016 BIS depht 25 m | | |
| | | | | | | | | NDT_20_2016 BIS depht 50 m | | |

| | | | | | | | | | | |
|---|---|---|---|---|---|---|---|---|---|---|
| | | | | | | | | NDT_20_2016 BIS depht 64 m | | |
| NDT_20_2016 BIS replica | 21/06/16 | 43°48'11,51 | 09°57'52,65 | 73 | | | | | 2 m | |
| NDT_20_2016 BIS SW104 | 21/06/16 | 43°48'11,66 | 09°57'52,68 | 73 | X | | | (Acqua interfaccia) | 1,25 m | |
| NDT_20_2016 BIS SW104 replica | 21/06/16 | 43°48'11,66 | 09°57'52,68 | 73 | | | | | 1,10 m | |
| NDT_22_2016 | 21/06/16 | 43°49'14,96 | 09°35'19,99 | 436 | X | X | | NDT_22_2016 depht 5 m | 3,20 m | A-D |
| | | | | | | | | NDT_22_2016 depht 50 m | | |
| | | | | | | | | NDT_22_2016 depht 100 m | | |
| | | | | | | | | NDT_22_2016 depht 300 m | | |
| | | | | | | | | NDT_22_2016 depht 410 m | | |
| NDT_22_2016 SW104 | 21/06/16 | | | 436 | X | | | (Acqua interfaccia) | 1,29 m | |
| NDT_22_2016 SW104 replica | 21/06/16 | | | 436 | | | | | 0,76 m | |
| MPS_13_2016 | 21/06/16 | N 43°45'25,50 | E 09°02'26,05 | 1460 | | | X | | | |
| NDT_25_2016 | 22/06/16 | 43°32'59,82 | 08°50'16,33 | 2294 | X | X | | NDT_25_2016 depht 45 m | 4,78 m | A-E |
| | | | | | | | | NDT_25_2016 depht 140 m | | |
| | | | | | | | | NDT_25_2016 depht 350 m | | |
| | | | | | | | | NDT_25_2016 depht 580 m | | |
| | | | | | | | | NDT_25_2016 depht 1000 m | | |
| | | | | | | | | NDT_25_2016 depht 2264 m | | |
| MPS_13_2016 replica | 22/06/16 | N 43°45'23,81 | E 09°02'19,55 | 1460 | | | X | | | |
| NDT_23_2016 | 22/06/16 | 44°02'03,73 | 09°25'37,40 | 531 | X | X | | NDT_25_2016 depht 70 m | 3 m | A-C |
| | | | | | | | | NDT_25_2016 depht 140 m | | |
| | | | | | | | | NDT_25_2016 depht 270 m | | |
| | | | | | | | | NDT_25_2016 depht 505 m | | |
| NDT_23_2016 SW104 | 22/06/16 | 44°02'03,56 | 09°25'37,62 | 531 | X | | | (Acqua interfaccia) | 1,15 m | |
| NDT_23_2016 SW104 replica | 22/06/16 | 44°02'03,56 | 09°25'37,62 | 531 | X | | | | 0,89 m | |
| MPS_13_2016 BIS | 23/06/16 | N 42°46'25,02 | E 09°51'41,12 | 495 | | | X | | | |
| NDT_28_2016 | 23/06/16 | N 40°55'49,12 | E 10°37'26,5 | 2323 | | X | | NDT_28_2016 depht 50 m | | |
| | | | | | | | | NDT_28_2016 depht 100 m | | |
| | | | | | | | | NDT_28_2016 depht 240 m | | |
| | | | | | | | | NDT_28_2016 depht 400 m | | |
| | | | | | | | | NDT_28_2016 depht 1000 m | | |
| | | | | | | | | NDT_28_2016 depht 2293 m | | |
| NDT_30_2016 | 24/06/16 | N 38°47'00,93 | E 10°42'26,38 | 2437 | | X | | NDT_30_2016 depht 25 m | | |
| | | | | | | | | NDT_30_2016 depht 60 m | | |
| | | | | | | | | NDT_30_2016 depht 100 m | | |
| | | | | | | | | NDT_30_2016 depht 300 m | | |
| | | | | | | | | NDT_30_2016 depht 1000 m | | |
| | | | | | | | | NDT_30_2016 depht 2409 m | | |
| NDT_6_2016 | 25/06/16 | N 38°00'00,05 | E 11°47'00,05 | 1066 | X | X | | NDT_6_2016 depht 25 m | 4,14 m | A-E |
| | | | | | | | | NDT_6_2016 depht 400 m | | |
| | | | | | | | | NDT_6_2016 depht 1036 m | | |
| NDT_6_2016 SW104 | 25/06/16 | N 37°59'59,75 | E 11°46'59,77 | 1066 | X | | | (Acqua interfaccia) | 1,26 m | |
| NDT_6_2016 SW104 replica | 25/06/16 | N 37°59'59,76 | E 11°46'59,78 | 1066 | | | | | 1,32 m | |
| MPS_4_2016 | 25/06/16 | 37°59'57,53 | 11°47'23,61 | 1062 | | | X | | | |
| NDT_32_2016 | 25/06/16 | 39°10'35,12 | 12°13'01,08 | 3509 | | X | | NDT_32_2016 depht 115 m | | |
| | | | | | | | | NDT_32_2016 depht 375 m | | |
| | | | | | | | | NDT_32_2016 depht 1125 m | | |
| | | | | | | | | NDT_32_2016 depht 3477 m | | |
| NDT_6BIS_2016 | 26/06/16 | 38°16'57,50" | 12°44'29,08 | 873 | | X | | NDT_6BIS_2016 depht 40 m | | |
| | | | | | | | | NDT_6BIS_2016 depht 80 m | | |
| | | | | | | | | NDT_6BIS_2016 depht 427 m | | |
| | | | | | | | | NDT_6BIS_2016 depht 844 m | | |
| NDT_6TER_2016 | 26/06/16 | 38°16'14,89 | 12°54'27,37 | 1045 | | X | | | | |
| MPS_5_2016 BIS | 27/06/16 | 38°14'24,67 | 13°45'14,78 | 1372 | | X | | | | |